742 *Biochemistry* **2010,** *49,* 742–751
DOI: 10.1021/bi901536j

BIOCHEMISTRY
including biophysical chemistry & molecular biology
Article

Differences in the Molecular Structure of β_2-Microglobulin between Two Morphologically Different Amyloid Fibrils[†]

Hirotsugu Hiramatsu,[‡,⊥] Ming Lu,[‡,@] Koichi Matsuo,[§] Kunihiko Gekko,[§] Yuji Goto,[∥] and Teizo Kitagawa*[,‡,#]

[‡]*Okazaki Institute for Integrative Bioscience, National Institutes of Natural Sciences, Okazaki 444-8787, Japan,* [§]*Graduate School of Science, Hiroshima University, Higashi-Hiroshima 739-8526, Japan, and* [∥]*Institute for Protein Research, Osaka University, 3-2 Yamadaoka, Suita, Osaka 565-0871, Japan.* [⊥]*Present address: Graduate School of Pharmaceutical Sciences, Tohoku University, Aobayama, Sendai 980-8578, Japan.* [@]*Present address: Key Laboratory for Molecular Enzymology and Engineering, Ministry of Education, Jilin University, Changchun, Jilin 130021, P. R. China.* [#]*Present address: Toyota Physical and Chemical Research Institute, Nagakute, Aichi 480-1192, Japan.*

Received September 2, 2009; Revised Manuscript Received November 25, 2009

ABSTRACT: Differences in the molecular structures of β_2-microglobulin between the two morphologically different amyloid fibrils having a needlelike [long−straight (LS)] and flexible [wormlike (WL)] character were investigated by infrared, Raman, and vacuum−ultraviolet circular dichroism spectroscopy. It turned out that although the β-sheet content was comparable between the two kinds of fibrils (53 ± 6% for the LS fibril and 47 ± 6% for the WL fibril), the protonation states of the carboxyl side chains were distinctly different; the deprotonated (COO^-) and protonated (COOH) forms were dominant in the LS and WL fibrils at pH 2.5, respectively, meaning that the pK_a is specifically lowered in the LS fibril. Such a difference was not observed for the fibrils of the core fragments. Since site-specific interactions generally cause variation in the pK_a of carboxyl side chains in proteins, these results suggest that "hook"-like interactions generated by hydrogen bonding and the formation of a salt bridge are present in the LS fibril, providing enthalpic stabilization. Presumably, the carboxyl groups fix the spatial arrangement of β-strands and β-sheets, bringing about the needlelike morphology. The absence of this regulation would result in the flexible morphology of the WL fibril, providing entropic stabilization.

β_2-Microglobulin (β_2m)[1] is a light chain of the class I major histocompatibility complex. It consists of 99 residues and contains two β-sheets bound with a disulfide bond (immunoglobulin fold) (*1*). The formation of amyloid fibrils occurs in patients undergoing dialysis, and its deposition in tissues is the cause of several disorders (dialysis-related amyloidosis).

There are two fundamental issues to be clarified with regard to the fibril formation of β_2m. (i) Why are fibrils formed under physiological conditions in vivo (fibril formation is known to take place under acidic conditions or with the aid of several compounds in vitro)? (ii) What is the thermodynamically most stable protein structure in the fibril under the given conditions? Such issues are general, and not specific to β_2m. The first question is related to the idea that "the protein structure in the native state is unique and thermodynamically most stable under the physiological conditions" (Anfinsen's dogma). Spontaneous fibril formation implies that the fibril state is expected to be more stable than the soluble monomer state for these very reasons.

For β_2m, the effects of additional factors such as Cu^{2+} (*2*, *3*), sodium dodecyl sulfate (*4*), collagen (*5*, *6*), and nonesterified fatty acids (*7*) have been reported to lower the stability of the native state at neutral pH, suggesting that these factors induce the transformation of β_2m from the native state to an intermediate state directed toward fibrillization. It is considered that an additional factor is indispensable under physiological pH, because this would be consistent with the dogma. Fibril formation also proceeds through an acid-denatured state (*8*−*10*), and in this case, protonation of the β_2m molecule is crucial. The effects of these factors on the protein secondary structure are also intriguing; the Cu^{2+} ions coordinate to the side chain of His31 and facilitate the cis−trans isomerization of Pro32, yielding the intermediate state (*2*, *3*). For SDS and collagen, charged groups are thought to play an essential role (*4*, *5*). The fatty acids are thought to partially unfold β_2m to an aggregation-prone conformer at neutral pH (*7*).

The second problem concerns the origin of the thermodynamic stability of the molecular structure of proteins in the fibril. At present, the determination of the atomic coordinates is still in progress. Furthermore, the reason for the morphological resemblance of the amyloid fibrils generated by different proteins also remains to be explained, since common features of both the protein secondary structures and fibril morphology have been commonly noted. The fibril adopts a linear morphology without branching (~10 nm in thickness and a few micrometers in length) irrespective of the precursor protein species, and it consists of several twisted thinner elements (called protofilaments) in most cases; the number of the protofilaments constituting a fibril and the period of internal twist were variable, even if the fibrils were

[†]This study was supported by JSPS Research Fellowships for Young Scientists to H.H. and by a Grant-in-Aid for Scientific Research (21350098) to T.K. from the Ministry of Education, Culture, Sports, Science and Technology of Japan.

*To whom correspondence should be addressed. E-mail: Riken-kitagawa@mosk.tytlabs.co.jp. Telephone: +81-80-1620-8159. Fax: +81-561-63-6302.

[1]Abbreviations: β_2m, β_2-microglobulin; β_2m_{21-29}, fragment of residues 21−29 of β_2-microglobulin; β_2m_{20-41}, fragment of residues 20−41 β_2-microglobulin; β_2m_{76-91}, fragment of residues 76−91 of β_2-microglobulin; K3, β_2m_{20-41} fragment; K7, β_2m_{76-91} fragment; Aβ_{1-40}, fragment of residues 1−40 of human amyloid β protein; WL, wormlike; LS, long−straight; AFM, atomic force microscopy; TEM, transmission electron microscopy.

 Published on Web 12/22/2009

formed under an identical condition (*11*), although the β-sheet core structure is commonly seen in fibrils (*12*).

Any factor that determines this linear morphology should be a fundamental property of amyloid proteins, because this is commonly observed, irrespective of the precursor protein. Elucidation of such a factor is one of purposes of this study, for which it is beneficial to compare the structures of the same protein in fibrils with different morphology. A few examples have already been reported; the $A\beta_{1-40}$ fibril displays a different morphology with regard to the periodic twist under quiescent and/or agitated conditions, and a structural difference was observed in the presence or absence of the salt bridge between Lys16 and Glu22 for these two morphologically different fibrils (*13*). In terms of the fibril of the K13A mutant of the $A\beta_{13-21}$ fragment, the concentration of Zn^{2+} ions rapidly brings about assembly of a helical ribbon instead of a fibril (*14*). Other examples include the aggregates of α-synuclein, the morphology of which depends on changes in the pH and salt concentration (*15*), and human stefin B, which is influenced by the pH condition and the concentration of 2,2,2-trifluoroethanol (*16*). Multiple morphologies appearing under different conditions of protein concentration, pH, and salt concentration have been reported for β_2m (*10*). In these studies, however, the molecular mechanism inducing the morphological difference and the relevance of the structural nature of proteins and/or peptides to a particular morphology have not been elucidated. Several imaging techniques, such as atomic force microscopy (AFM) (*11*, *17*), electron microscopy (*18*), and evanescent fluorescence microscopy (*19*, *20*), have been developed; a number of the morphological characteristics of the fibril have been identified, and the effects of mutation and/or chemical conditions on fibril morphology have come under investigation. In contrast, the forthcoming structural information has not been abundant, in part because of the difficulties in applying X-ray crystallography and NMR (*21*−*24*).

For our purposes, the β_2m fibril was targeted because the multiple morphologies and their formation conditions have been established (*10*) and the morphological differences of the β_2m fibril are clearest among those studied so far. Accordingly, the long−straight (LS) and wormlike (WL) fibrils of β_2m were treated in this study. The structural analysis of the fibril of the core fragment of β_2m has been reported (*24*). However, structural analysis of the fibril of large proteins by high-resolution techniques is still limited to date. We employed infrared absorption (IR), Raman scattering, and vacuum−ultraviolet circular dichroism (VUVCD) spectroscopy. IR and Raman spectroscopy have been widely applied to the structural analysis of biomolecules (*25*−*31*). The similarity and difference of the structural character of each fibril will be elucidated by direct comparison of IR spectra. Application of IR spectroscopy to the fibril structure is particularly advantageous because of the utilization of the ^{13}C isotope labeling technique (*32*−*34*) and linear dichroism measurement (*35*). CD spectroscopy is known as a powerful technique for secondary structure analysis (*36*), and its measurements, at shorter wavelengths in particular, are expected to increase the precision of the secondary structure determination. In this study, the measurement is extended to 172 nm with synchrotron radiation.

Structures of several states of β_2m fibrils have been investigated by using IR spectroscopy. Jahn et al. (*37*) demonstrated the structural identity between the LS fibrils prepared in vitro and in vivo and indicated the spectral difference of the LS fibril from the WL fibril and an amorphous aggregate. Fabian et al. (*38*) investigated the conformational changes associated with the assembly of β_2m under acidic conditions and pointed out structural differences between several states. They revealed that the heat-triggered conversion accompanied the morphological as well as the structural changes. Apart from their investigation, our study aims at a quantitative analysis of the secondary structure content and the protonation state of COOH groups.

Scheme 1

$^{-4}$EAYV
^{1}IQRTPKIQVYSRHPAENGKSNFLNCYVSGF
^{31}HPSDIEVDLLKNGERIEKVEHSDLSFSKDW
^{61}SFYLLYYTEFTPTEKDEYACRVNHVTLSQP
^{91}KIVKWDRDM

EXPERIMENTAL PROCEDURES

Sample Preparation. Recombinant β_2m from yeast (*Pichia pastoris*) was used in this study; four additional residues (Glu^{-4}-Ala^{-3}-Tyr^{-2}-Val^{-1}) were attached to the N-terminus (*8*). The sequence is shown in Scheme 1.

The needlelike fibril which appears long and straight was prepared by following the reported procedure (*8*). Briefly, β_2m was dissolved in buffer containing 50 mM citrate (pH 2.5) and 100 mM NaCl, and the protein concentration was adjusted to 84 μM (1.0 mg/mL). The preformed LS fibril was added as a seed (final concentration of 5 μg/mL), and then it was incubated at 37 °C for 10 h. Note that fibril formation occurs in two steps (nucleation and elongation), and the addition of the preformed fibril allows the former step (the seed effect) to be skipped. According to Gosal's diagram, the long−straight (LS) fibril is spontaneously formed under this condition without the seed (*10*), but slowly. The flexible fibril, which appears wormlike, was prepared according to the previous report (*9*, *39*). Briefly, β_2m was dissolved in buffer containing 50 mM citrate (pH 2.5) and 200 mM NaCl, and the protein concentration was adjusted to 42 μM (0.5 mg/mL) and then the mixture incubated at 37 °C for 1 week. According to Gosal's diagram, the wormlike (WL) fibril is expected to appear under this condition (*10*).

The structures of β_2m in the native and denatured states in solution were also examined and compared with those of the two fibrils. For IR and Raman spectroscopy, the native state of β_2m was prepared in buffer containing 50 mM phosphate (pH 7.5) and 100 mM NaCl, and the denatured state was prepared in buffer containing 50 mM citrate (pH 2.5) and 100 mM NaCl. The concentration of β_2m was adjusted to ca. 170 μM (2 mg/mL) in both cases. To avoid the interference from Cl^-, the salt concentration was changed only for the VUVCD measurements of the native and denatured states (see below).

Two peptide fragments having a partial sequence of β_2m were also treated in this study. Peptide fragment β_2m_{20-41} (denoted as K3) having a partial sequence of β_2m [^{20}SNFLNCYVSGFHPSDIEVDLLK^{41} (see Scheme 1)] (*40*) was synthesized at the National Institute for Basic Biology, Japan, Center for Analytical Instruments (Okazaki, Japan), purified by HPLC (Develosil ODS-HG-5 column, Nomura chemical), and stored as a DMSO solution (25 mg/mL) at −80 °C. The other peptide fragment, K3−K7 [cf. K7 = β_2m_{76-91} (^{76}DEYACRVNHVTLSQPK^{91}) bound to K3 with a disulfide bridge between Cys25 and Cys80 (see Scheme 1)],

was prepared by application of a lysyl endopeptidase (Wako Pure Chemical) to β_2m (*40*). It was purified by HPLC (Develosil ODS-HG-5 column, Nomura chemical) and stored as a DMSO solution (25 mg/mL) at −80 °C. These peptides were dissolved in the buffer (pH 2.5) containing 50 mM citrate and various concentrations of NaCl (see below) and were adjusted to a concentration of 100 μM. The solution was incubated at 37 °C for 10 h, and the fibril was obtained by spontaneous fibril formation.

Measurements. (*i*) *IR Spectroscopy*. IR spectra were recorded with an FT-IR microscope spectrometer (Avatar360 and Continuμm, Thermo Nicolet) with a transmission setup. Each spectrum presented was an average of 1024 spectra. The spectral resolution was 4 cm^{-1}. In the linear dichroism measurement, inaccuracy in the polarization of the probe light due to the solid angle of the focal objective Cassegrain mirrors (NA 0.65) of the IR microscope was compensated by taking the hole size of the iris into account (*41*).

The good correlation between the secondary structure of the peptide main chain and the peak position of the amide I band is well-known (*25*); the amide I bands of non-α-non-β (β-turn, loop, β-bulge, etc.), α-helix and random coil, and the β-sheet structures are expected to appear at >1660, 1660−1640, and 1640−1620 cm^{-1}, respectively. Also, the number of residues contained in each secondary structure is estimated from the ratio of the integrated band intensities, because it is nearly proportional to the number of peptide groups present. Thus, the secondary structure content was estimated for the fibrils on the basis of this principle.

Data sampling and handling were performed as reported previously (*42*). The structural analysis described here is based on the assumptions that (i) there is no exception in the empirical relationship between the amide I frequencies and the secondary structure and (ii) the molar extinction coefficient depends little on the secondary structures. These assumptions are acceptable because the secondary structure contents of several proteins tested agree well with those from X-ray crystallography, the deviation being 4% (*25*) or <5% (*26*).

In the band fitting analysis, the fitting parameters were chosen so that both the observed IR spectrum and its second-derivative spectrum could be reproduced simultaneously. As a result, the error was reduced to nearly 1% of the determined parameters in every case, and it was sufficiently smaller than the error of systematic uncertainty.

(*ii*) *VUVCD Spectroscopy*. Circular dichroism (CD) measurement has been extensively employed in the analysis of the secondary structure content of proteins (*36*), and the accuracy is improved when the spectrum is recorded at shorter wavelengths. One reason for this is that CD spectroscopy with vacuum−ultraviolet light (VUVCD) was employed.

The native state of β_2m was prepared in a buffer containing 50 mM phosphate (pH 7.5), while the acid-denatured state was prepared in a buffer containing 5 mM citrate (pH 2.5); the sample concentration was increased to 2.5 mg/mL (210 μM), while NaCl was not added to the VUVCD samples. The LS and WL fibril states were prepared as described for IR Spectroscopy.

The VUVCD spectra of β_2m in the native and acid-denatured states were measured from 172 to 260 nm under high vacuum (10^{-4} Pa) using the VUVCD spectrophotometer constructed at the Hiroshima Synchrotron Radiation Center (*43*) and an assembled-type optical cell (*44*). The VUVCD spectra of β_2m in the LS and WL fibrils were measured from 187 to 260 nm due to the disturbance by the absorption of Cl^- ions in the short wavelength region. The path length of the cell was adjusted with a Teflon spacer to 50 or 25 μm. All of the VUVCD spectra were recorded with a slit width of 0.25 mm, an instrument time constant of 16 s, a scan speed of 4 nm/min, and four to nine accumulations of spectra.

The secondary structure contents of β_2m in each state were analyzed using SELCON3 (*36*) and the VUVCD spectra of 12 reference proteins that are known to be rich in β-strand [the Protein Data Bank (PDB) entries are given in parentheses] (*45*, *46*): β-lactoglobulin (1B8E), pepsin (4PEP), trypsinogen (1TGN), α-chymotrypsinogen (2CGA), soybean trypsin inhibitor (1AVU), concanavalin A (2CTV), carbonic anhydrase (1G6V), elastase (3EST), avidin (1AVE), xylanase (1ENX), azurin (1E5Z), and β_2m (3HLA). To determine the secondary structures of these proteins in a crystal, the DSSP program (*47*) was employed.

The VUVCD data allow the determination of the contents of "regular α-helix" (α_R), "distorted α-helix" (α_D), "regular β-sheet" (β_R), "distorted β-sheet" (β_D), "turn", and "unordered" structures. Four residues of the α-helix and two residues of the β-strand at their termini (the "distorted α-helix/β-strand") were postulated to appear with a pattern different from that of the remaining parts (the "regular α-helix/β-strand") in the CD spectrum (*48*), and accordingly, they are distinguishable. The secondary structure contents of the α-helix, β-sheet, and others were calculated from $\alpha_R + \alpha_D$, $\beta_R + \beta_D$, and the fraction of turn and unordered structures, respectively. Besides the secondary structure contents, the number of segments is another parameter used to characterize the α-helix and β-sheet structures in proteins. For example, myoglobin consists of eight segments of the α-helix, and β_2-microglobulin consists of seven segments of the β-strand. The number of α-helix segments (N_α) was determined using the equation $N_\alpha = (\alpha_D N_{res})/4$, and the number of β-strand segments (N_β) was determined using the equation $N_\beta = (\beta_D N_{res})/2$, where α_D and β_D are the fraction of distorted α-helix and distorted β-strand, respectively, and N_{res} is the number of residues in β_2m.

With regard to the systematic errors, the estimated discrepancy between VUVCD spectroscopy and X-ray crystallography is 6.6% for the α-helix, 9.8% for the β-sheet, and 8.1% for the others. The root-mean-square deviation (δ) and the correlation coefficient (r) of the number of the segments were 2.4 and 0.75 for the α-helix and 2.9 and 0.88 for the β-strand, respectively (*46*). It is worth noting that r for the β-strand is larger than that for the α-helix in our analysis because an appropriate reference protein set was chosen. The uncertainty of the fitting parameters, which was nearly 1% of the determined values, was smaller than the systematic error.

(*iii*) *Raman Spectroscopy*. Raman spectra were excited at 488 nm with an Ar^+ ion laser (NEC) and recorded as described previously (*33*). The reproducibility of the peak positions was within 1 cm^{-1}.

(*iv*) *Electron Microscopy*. The prepared fibrils dispersed in the solution were diluted 20-fold with pure water. An aliquot (5 μL) of the diluted solution was placed on a copper grid (400 mesh) covered by a carbon-coated collodion film for 60 s. Excess sample solution was removed by blotting with a filter paper. The sample was negatively stained with a 2% (w/v) uranyl acetate solution for a further 60 s. The liquid on the grid was blotted again with a filter paper and air-dried. For the LS fibril, images were recorded using an H-7000 electron microscope (Hitachi) with an acceleration voltage of 75 kV at the Research Center for Ultrahigh Voltage Electron Microscopy at Osaka University. The magnification was 30000×.

Images of the other samples were taken using a JEM1200EX (JEOL) transmission microscope with an acceleration voltage of 80 kV. The magnification was 30000×.

(*v*) *Atomic Force Microscopy*. An aliquot (15 μL) of the prepared fibrils dispersed in the solution (those of LS and WL fibrils were diluted 20- and 10-fold with pure water, respectively) was put on a mica plate, and an excess amount of the buffer was removed after a few minutes. The fibril was rinsed with pure water (20 μL) and dried. On this sample, AFM images were acquired using a Digital Instruments Nanoscope IIIa scanning microscope at 25 °C (Veeco, Tokyo, Japan). Measurements were performed using an air tapping mode.

RESULTS

Native, Acid-Denatured, and Fibril States of β_2m. (*i*) *Native and Acid-Denatured Solution States of β_2m.* The IR spectrum of β_2m in the native state at pH 7.5 is shown by the thick solid line in Figure 1a, in which the amide I and II bands are observed at ca. 1630 and ca. 1550 cm^{-1}, respectively. The fitted spectrum and the decomposed bands are also depicted in Figure 1a by the dotted and thin solid lines, respectively. The percentages of secondary structure content equal to the proportion of the number of residues in each of the secondary structures of the 103 residues (see Scheme 1) deduced from the intensities of the corresponding bands are listed in Table 1, where the α-helix and random coil structures are not discernible, because both give the amide I band at nearly the same frequency (1640−1660 cm^{-1}). Therefore, the contents of the α-helix and random coil structures were not determined separately. The content of all but the β-sheet structure in the native state is placed in the column of "nonregular" structures in Table 1 for the sake of simplicity, although the α-helix in fact is a regular structure.

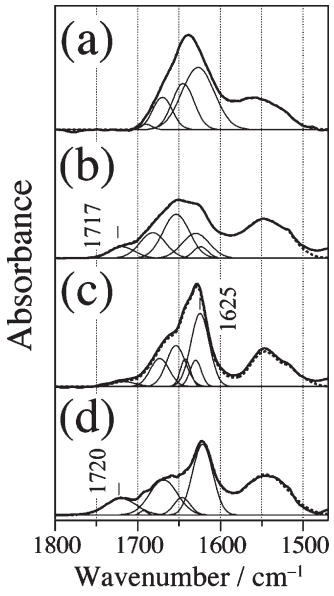

FIGURE 1: IR spectra of the β_2m monomer in solution at pH 7.5 (a) and 2.5 (b) and of the LS fibril at pH 2.5 (c) and the WL fibril at pH 2.5 (d). Observed spectra (solid lines), fitted results (dashed lines), and decomposed bands (thin solid lines) are depicted for panels a−d. The traces are normalized by taking into account the area in the 1470−1800 cm^{-1} region.

The VUVCD spectrum of the native state, which is shown by a thick solid line in Figure 2, exhibited an undulation curve in the 200−260 nm region and a large negative peak at 175 nm, with a shoulder around 185 nm. This is a typical pattern for proteins having a β-barrel structure such as avidin (*46*) and Bence-Jones protein (*49*). The secondary structure content as well as the numbers of segments of the α-helix and β-strand was deduced from these spectra, as shown in Table 1.

The Raman spectrum of the native state of β_2m is shown in Figure 3a. As for the IR spectra, the empirical relations between the amide I frequencies and the secondary structures of proteins are well-established in Raman spectra (*28*). The α-helix, β-sheet, and random coil structures yield bands at ∼1655, ∼1670, and ∼1660 cm^{-1}, respectively. It is noted that the Raman frequencies

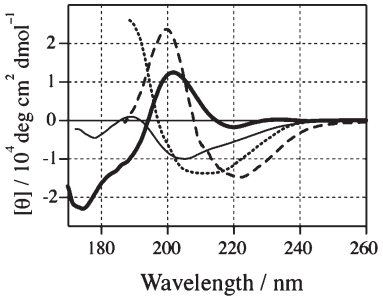

FIGURE 2: VUVCD spectra of β_2m in solution at pH 7.5 (thick solid line) and 2.5 (thin solid line) and of the LS fibril at pH 2.5 (dashed line) and the WL fibril at pH 2.5 (dotted line).

Table 1: Secondary Structure Content of β_2-Microglobulin

			secondary structure content (%)		
state	pH	method	α-helix	β-sheet	nonregular
native	7.5	IR	—	55	45[d]
	7.5	VUVCD[a]	−0.9 (0.2) [α_R −1.5, α_D 0.6]	50.4 (6.3) [β_R 38.1, β_D 12.3]	51.7 [turn 23.8, unordered 27.9]
	7.75	CD[b]	0	59	41
	5.7	X-ray[c]	0.0	49.5	50.5
denatured	2.5	IR	—	32	69[d]
	2.5	VUVCD[a]	13.5 (2.6) [α_R 3.3, α_D 10.2]	34.4 (7.1) [β_R 20.6, β_D 13.8]	55.4 [turn 22.1, unordered 33.3]
LS fibril	2.5	IR	—	51	49[d]
	2.5	VUVCD[a]	1.4 (0.2) [α_R 0.7, α_D 0.7]	54.2 (7.6) [β_R 39.4, β_D 14.8]	46.6 [turn 23.6, unordered 23.0]
WL fibril	2.5	IR	—	53	47[d]
	2.5	VUVCD[a]	20.5 (2.8) [α_R 9.7, α_D 10.8]	41.9 (6.1) [β_R 30.1, β_D 11.8]	40.3 [turn 20.1, unordered 20.2]

[a]Values in parentheses denote the number of segments having the secondary structure. See the text. [b]From ref *26*. [c]From ref *1*. [d]α-Helix is included (see the text).

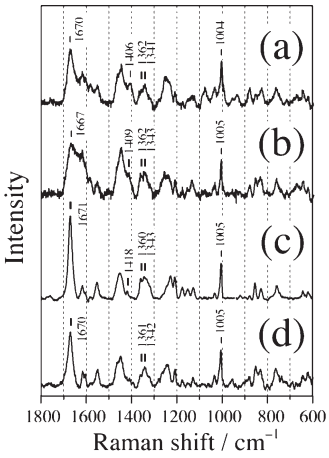

FIGURE 3: Raman spectra of β_2m in the native (a), denatured (b), LS fibril (c), and WL fibril (d) states. Spectra were recorded with excitation at 488 nm and were normalized by the band intensity of phenylalanine at 1005 cm^{-1}.

of each secondary structure are different from those in the IR spectrum because of differences in the selection rule. The Raman amide I band of β_2m in the native state appeared strongly at 1670 cm^{-1}, indicating the dominance of the β-sheet structure.

Taking into account the average of the results of IR and VUVCD spectroscopy [55 ± 5 and 50.4 ± 9.8%, respectively (see Table 1)], we determined the β-sheet content of β_2m in the native state to be 53 ± 6%. This is in good agreement with the β-sheet content deduced from X-ray crystallography (49.5%) (*1*) and ordinary CD spectroscopy (59%) (*50*) within the margin of error. The absence of an α-helix and the deduced number of β-strand segments (6.3 ± 2.9) are in agreement with the literature values (*1*). Thus, the β-sheet content of β_2m in the native solution state was established.

Next, the acid-denatured state of β_2m was examined. The observed IR spectrum (Figure 1b), the VUVCD spectrum (thin solid line in Figure 2), and the Raman spectrum (Figure 3b) were analyzed, and the secondary structure content and the number of the segments deduced are summarized in Table 1; the estimated β-sheet content was 32 ± 5% by IR and 34.4 ± 9.8% by VUVCD. The lowering of the β-sheet content in the denatured state (33 ± 6% on average) is consistent with a reported transformation from the β-sheet to randomness in a partially denatured state at pH 3.6 (*51*). An increase in the number of β-strand segments (from 6.3 to 7.1) is accompanied by a decrease in β-sheet content.

The α-helix structure was present in the acid-denatured state, as shown by the fact that both the content of the α-helix structure (13.5 ± 6.6%) and the number of α-helix segments (2.6 ± 2.4) were beyond the margin of error. This conclusion is in agreement with the result from NMR spectroscopy that demonstrated a decrease in β-sheet content and an increase in α-helix content in the acid-denatured state at pH 2.5 (*52*). The NMR study assigned 11 residues from Lys58 to Thr68 (10% of 99 residues) to the α-helix, in agreement with the result presented here.

The band broadening to the low-frequency side of the amide I band at 1667 cm^{-1} in the Raman spectrum (Figure 3b) suggested an increase in the content of α-helix (1655 cm^{-1}) and/or random (1660 cm^{-1}) structures. This agreed with the result of VUVCD spectroscopy. Besides the amide I band, other bands observed in the IR and Raman spectra can be used for the analysis of the side chain structures. We analyzed the structure of the carboxyl group

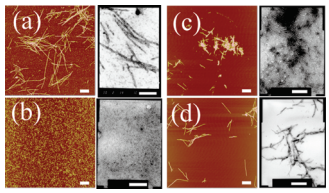

FIGURE 4: AFM (left) and TEM (right) images of amyloid fibrils: (a) β_2m LS fibril, (b) β_2m WL fibril, (c) K3 fibril, and (d) K3−K7 fibril. The scale bar in each image is 0.5 μm.

from the intensity of the C=O stretching band of COOH groups at 1715−1740 cm^{-1} on the IR spectrum (*30*, *53*), and the COO^- antisymmetric stretching band of COO^- groups around 1415 cm^{-1} on the Raman spectrum (*54*).

At pH 7.5, the C=O stretching band of COOH is not present around 1715−1740 cm^{-1} on the IR spectrum (Figure 1a), and the COO^- stretching band is observed at 1406 cm^{-1} on the Raman spectrum (Figure 3a). This means that the carboxyl side chains of β_2m in the native state mainly exist in the COO^- form. This result is reasonable because the carboxyl groups are located on the surface of the protein (*1*), and the pK_a of the side chains of Asp and Glu is approximately 3−5 (*55*). In the acid-denatured state at pH 2.5, on the other hand, most of the carboxyl groups of β_2m are protonated, because a large band of COOH was observed at 1717 cm^{-1} on the IR spectrum (Figure 1b) and the Raman band of the COO^- group at 1409 cm^{-1} became weaker (Figure 3b). Since these bands must be due to the side chains of Asp and Glu, these groups are presumably exposed to the solvent under this condition.

The intensity ratio of the Raman bands of Trp at 1340 and 1360 cm^{-1} (Trp doublet) serves as an indicator of the hydrophobicity of the environment around the Trp side chain (*56*); the ratio (I_{1360}/I_{1340}) becomes larger for more hydrophobic environments, and this relationship holds when the Raman spectrum is measured in the nonresonant condition. β_2m has two Trp residues (Trp60 and Trp95). Trp60 is exposed to the solvent, but Trp95 is buried in the native state (*1*). It is likely that the ratio of the doublet bands at 1340 and 1360 cm^{-1} in Figure 3a (ratio of 0.6) corresponds to the relatively exposed state. Under the acidic condition (pH 3.6), the conformation of the C-terminal region of the partially denatured β_2m, including Trp95, turned into a random coil (*51*), and this transformation exposed the Trp95 side chain to the solvent. The increase in the intensity ratio of the doublet bands (ratio of 0.9) is reasonably explained by taking this structural change into account.

The intensity ratio of the Raman bands of Tyr at 850 and 830 cm^{-1} (Tyr doublet) is known to be an indicator of the hydrogen bonding of the Tyr side chain (*57*). The hydrogen bonds of each Tyr residue, however, cannot be identified from the ratio, because seven Tyr residues are present in this protein (see Scheme 1). In this way, the conclusions obtained with these methods about the structure of the native and acid-denatured states of β_2m in solution are in good agreement with those previously obtained with other techniques.

(*ii*) *LS and WL Fibril States of β_2m*. Structural analyses of β_2m in the LS and WL fibril states are described next. Atomic force microscope and transmission electron microscope images of the LS fibril are shown in the left and right panels of Figure 4a, respectively, and those of the WL fibril are shown in the left and right panels of Figure 4b, respectively. The scale bars are 0.5 μm. These images show that the prepared fibrils reveal the typical

features of the long−straight and wormlike fibrils, which are consistent with those in the previous reports (*8*−*10*, *39*). The IR, VUVCD, and Raman spectra of the LS fibril state are depicted in Figure 1c, the dashed line in Figure 2, and Figure 3c, respectively. The spectra of the WL fibril state are also shown in Figure 1d, the dotted line in Figure 2, and Figure 3d, respectively. We attempted to record the VUVCD spectra of the fibrils in the shorter wavelength region by removing the salt after the formation of fibrils. However, the desalting caused degradation of the LS fibrils, and the measurement was not successful. The average values of the estimated β-sheet content (Table 1) were 53 ± 6% in the LS fibrils and 47 ± 6% in the WL fibrils. Because the β-sheet content was comparable between the fibril and native states, the secondary structure preference was considered to be similar between them. In other words, the secondary structure in the fibril was not exceptional among the amyloid proteins in solution.

The VUVCD spectrum indicated that the α-helix structure present in the denatured state disappeared upon formation of the LS fibril. On the other hand, α-helix structure was found in the WL fibril (20.5 ± 6.6%); there was no information about which sequence formed the α-helix. The α-helix content in the WL fibril might be < 20.5%, because the intensity of the Raman band of the α-helix at 1655 cm^{-1} (Figure 3d) was weaker than expected. The presence of the α-helix in amyloid fibrils might be exceptional, but it is reported to be present [e.g., CAD domain of caspase-activated deoxyribonuclease (*58*)].

Most of the carboxyl groups of β_2m in the LS fibril exist in the deprotonated (COO^-) form, because an IR absorption band of COOH at 1715−1740 cm^{-1} was absent (Figure 1c) and a Raman band of COO^- was observed at 1418 cm^{-1}, although it was weak (Figure 3c). This result suggests that the carboxyl side chains were hidden from the solvent and their pK_a values were lower than the ordinary values for some reason. For the WL fibril, on the other hand, as the C=O band appeared at 1720 cm^{-1} with a strong intensity in the IR spectrum (Figure 1d) and the COO^- antisymmetric stretching band was very weak at ~1415 cm^{-1} in the Raman spectrum (Figure 3d), the carboxyl groups would be exposed to the solvent, as was the case in the denatured state.

Since the intensity ratio of the Trp doublet in the LS fibril (ratio of 0.9) was comparable to that in the acid-denatured state (ratio of 0.9), the environment of Trp residues in the LS fibril (Figure 3c) and that in the acid-denatured state (Figure 3b) are thought to be similar. Therefore, it is deduced that both the Trp60 and Trp95 side chains are exposed to the solvent. In consonance with this result, rapid H−D exchange was observed in the main chain of these residues in the LS fibril (*59*). The intensity ratio of the Trp doublet of the WL fibril [ratio of 0.6 (Figure 3d)] was close to that of the native state [ratio of 0.6 (Figure 3a)]. Accordingly, one of the two Trp residues would probably be placed in the hydrophobic environment in the WL fibril, although no information is available on which one it is.

We also measured IR linear dichroism of an oriented sample of the LS fibril, and the results are shown in Figure 5. In this experiment, the IR spectra were recorded by using two polarized IR beams with polarization at right angles with each other. The direction of polarization along which the amide I band at 1625 cm^{-1} yielded the largest intensity was defined as being in a "parallel" direction with regard to the fibril long axis, since the carbonyl groups in the β-sheet structure in the fibril were considered to be directed along the long axis of the fibril. The other polarization was regarded as being in the "perpendicular" direction. In

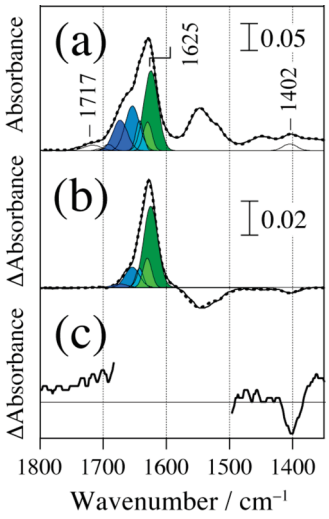

FIGURE 5: IR absorption (a) and linear dichroism (parallel − perpendicular) (b) spectra of the LS β_2m fibril. The results from band decomposition treatment are also depicted therein by using a fitted curve (dotted lines) and decomposed bands (colored). The bands colored green are assigned to the β-sheet, and those colored blue are assigned to the others. Trace c illustrates the experimental result in panel b with 10-fold magnification.

Table 2: Structural Parameters of LS Fibrils Deduced from IR Linear Dichroism Spectra[a]

position (cm^{-1})	assignment	content (%)	dichroic ratio R	α (deg)
1717	COOH (C=O stretch)	—	1.01	54
1692	Asn and Gln (C=O stretch)	—	0.96	60
1673	non-α-non-β	17	1.04	50
1654	random	24	1.16	37
1643	random	8	1.23	30
1630	β-sheet	9	1.39	0
1625	β-sheet	42	1.39	0
1402	C_α−H bend, CH_3 symmetrical bend, NH in-plane bend, C_α−C stretch	—	0.76	90

[a]Values of observed dichroic ratio R ($= A_\parallel/A_\perp$) are related to the angle α between the orientation axis and the direction of the transition dipole moment of the vibrational mode and also to the order parameter f (fraction of the completely aligned sample) by the following equation (*41*):

$$R(\alpha,f) = [f\cos^2 a + {}^1/_3(1-f)]/[{}^1/_2 f\sin^2\alpha + {}^1/_3(1-f)]$$

For the band that appeared with the largest dichroism (1625 cm^{-1}), the direction of the transition dipole moment was thought to be parallel to the fibril long axis (i.e., α was regarded to be 0°), and the parameter f was deduced from the observed value of R (= 1.39) to be 0.11. Then the α angles of the other bands were calculated with the f value and observed R values.

Figure 5a, the observed spectrum and the results of the fitting analysis are depicted with the solid and dotted lines, respectively. The decomposed components of the amide I band are also shown. The bands colored green were assigned to the β-sheet structure, and those colored blue were assigned to the other secondary structures. The difference spectrum (parallel − perpendicular) of the IR linear dichroism measurement is illustrated in Figure 5b; the observed spectrum, the results of fitting analysis, and the decomposed components of the amide I band are depicted in the same manner as in Figure 5a. A positive peak appears in the amide I region, suggesting that the transition

dipole moment of the amide I band is parallel to the fibril long axis. The negative peak appears in the amide II region (~1550 cm^{-1}) in Figure 5b, suggesting that the transition dipole moment of this mode is perpendicular to the long axis. Figure 5c shows the 10-fold magnified trace of the observed spectrum in Figure 5b (the middle of the trace was eliminated for the sake of simplicity).

The information about the angle (termed α) between the orientation axis of the LS fibril (the long axis of the fibril in this case) and the transition dipole moments of the mode was estimated from this experiment (see the footnote of Table 2 for calculations) (*35*). Note that the bands at 1640−1660 cm^{-1} were tentatively assigned to the random coil structure in Table 2, because the α-helix content was zero as determined by VUVCD spectroscopy (see Table 1).

Among the component bands of amide I, the band at 1625 cm^{-1} exhibited the largest dichroic ratio (R = 1.39). Since the largest dichroism should arise from the smallest α angle, the α value of this band was tentatively set to zero. The order parameter f regarding the fibril orientation was determined with this band, and the equation is presented in the footnote of Table 2. Although the f value (=0.11) of the sample presented here thus determined is not sufficiently high, the dichroism difference spectrum reflects only the aligned portion, because the spectra of the nonaligned portions are canceled in the difference calculations. Therefore, the discussion of the aligned moiety is qualitatively justified despite the small f value. The values of α were determined for the remaining bands as shown in Table 2. Accordingly, the α value of the LS fibril was 0°, indicating that the peptide C=O groups in the β-sheet core of the LS fibril were parallel with the fibril long axis. The deviation of α toward random structures (=54.7°) probably reflects the extent of flexibility.

We attempted to obtain some information about the orientation of the carboxyl groups from Figure 5c. The bands at 1692 and 1717 cm^{-1} were assigned to the C=O stretching of the Asn and Gln side chains and the COOH groups of Asp and Glu and the C-terminus, respectively (*53*). The α angles of these bands were determined from the dichroic ratio to be 54° and 60°, respectively, which are very close to the value of 54.7° expected for a random orientation. A weak band was observed at 1402 cm^{-1} in Figure 5a, for which two assignments were possible: the COO^- antisymmetric stretching band of the carboxyl groups in the deprotonated form (*30*) and a mixed mode of the peptide main chain in the β-strand, C_α−H bend, CH_3 symmetrical bend, NH in-plane bend, and C_α−C stretch (*60*). The transition dipole moment of the latter is known to be perpendicular to the peptide C=O groups in the β-strand. The negative peak in the difference spectrum (Figure 5c) indicates that the transition dipole moment of this mode is perpendicular to the fibril long axis, and therefore, the latter assignment is reasonable.

Another kind of oriented fibril samples was examined to confirm this assignment, that is, β_2m_{21-29}, a nine-residue peptide having a partial sequence of β_2m (Asn21−Gly29) and the fibril formation propensity. The propensity remained even when the electric charges on both termini were blocked. The polarized IR spectrum and the polarization difference spectrum of the LS fibril of β_2m_{21-29} are depicted in panels a and b of Figure 6, respectively. As no carboxyl group is contained therein, these spectra helped us to assign the band at 1402 cm^{-1}. An absorption band is present at 1396 cm^{-1} in the IR spectrum (Figure 6a), and the negative peak appears at the same position in the polarization difference spectrum (Figure 6b). This demonstrates that the IR band of the LS fibril at 1402 cm^{-1} should be assigned to the

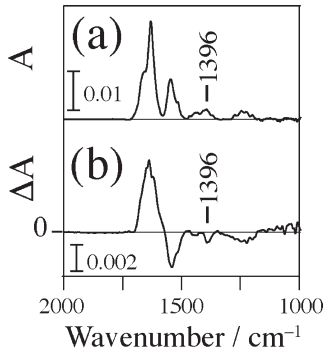

FIGURE 6: IR absorption (a) and linear dichroism (parallel − perpendicular) (b) spectra of the fibril of the β_2m_{21-29} fragment, the N- and C-termini of which are blocked with the acetyl and amide groups, respectively.

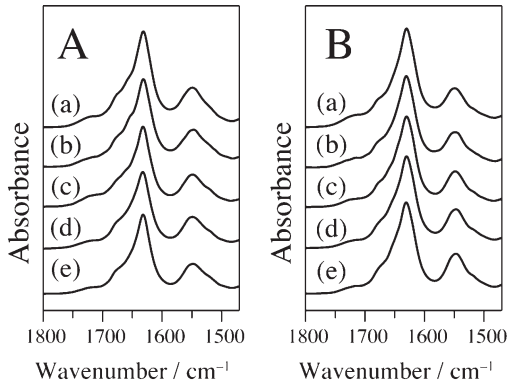

FIGURE 7: Salt concentration dependence of the IR spectra of the amyloid fibril of the (A) K3 and (B) K3−K7 fragments prepared at pH 2.5. The concentration of NaCl is set to (a) 0, (b) 20, (c) 100, (d) 200, or (e) 500 mM.

peptide main chain rather than to the COO^- groups. Thus, the information about the orientation of the COO^- groups could not be obtained from this band.

Preparation of oriented samples of the WL fibril was not successful because of the flexible morphology. Although very small particles having partial orientation might have formed, they were not detected with our IR microscope (its spatial resolution is worse than 10 μm), and therefore, we failed to measure the linear dichroism.

Fibrils of Short Peptide Fragments. Lowering the pK_a value of COOH groups was observed upon the formation of fibrils of the β_2m intact protein. The question of whether this phenomenon was also seen in fibrils with shorter peptide fragments arose. Figure 7 illustrates the salt concentration dependence of the IR spectra of K3 (A) and K3−K7 (B) fibrils, partial sequences of β_2m [K3 = β_2m_{20-41} and K7 = β_2m_{76-91} (see Scheme 1); Cys25 and Cys80 are bridged in the K3−K7 fragment]. These peptide fibrils provide the LS morphology at pH 2.5 as demonstrated in Figure 4c,d, where the scale bars is 0.5 μm. This observation is consistent with the previous report (*40*). The carboxyl groups of Asp34, Glu36, and Asp38 are contained in K3 and those of Asp76 and Glu77 in K7. With regard to the salt concentration dependence (0−500 mM) of the K3 (A) and K3−K7 (B) fragments, no special features were observed in the IR spectra at pH 2.5 (Figure 7), in contrast to the β_2m fibrils, indicating that the secondary structure content as well as the pK_a of the carboxyl groups was independent of the salt concentration in the cases of the short peptides.

DISCUSSION

The structures of β_2m in the two amyloid fibrils having distinct morphological appearances were investigated by means of IR, Raman, and VUVCD spectroscopy. The most remarkable difference was found in the protonation state of the carboxyl groups; at pH 2.5, most of the carboxyl groups were deprotonated in the LS fibril, while they were protonated in the WL fibril. In other words, the effective pK_a of the carboxyl side chains was much lower in the LS fibril than in the WL fibril. Such lowering of the pK_a of carboxyl groups occurs in a protein as a result of a change in the electrostatic potential, intramolecular hydrogen bonds, burial in a specific cavity (and consequent interaction with polar groups), etc. (*55*). Therefore, the structure and environment of the carboxyl groups in the LS fibril are considered to be very different from those in the WL fibril, the latter of which would be exposed to the solvent.

A plausible explanation is that the deprotonated carboxyl groups are surrounded by polar groups and stabilized by attractive interactions such as hydrogen bonding and salt bridges with them in the LS fibril. The lowering of the pK_a occurs in such cases; for example, the pK_a of Asp93 in barnase is less than 2.0 due to a semiburied salt bridge between Asp93 and Arg69 (*61*), and the pK_a of a deeply buried acidic residue in ribonuclease HI, Asp148, is less than 2.0 because of an ionic interaction network with Arg46 and Asp102 (*62*). The high susceptibility of the fibril morphology to the salt concentration (*10*) suggests the importance of the electrostatic interaction. This attractive interaction could be regarded as a "hook" between two residues, because it is powerful but rarely formed unless the partner residue comes into acceptable proximity. In contrast, hydrophobic interactions work nonspecifically between any hydrophobic residues. Thus, the importance of the hook-type interaction in the LS fibril is understood in terms of enthalpic stabilization, but the WL fibril stays in a stable state in the entropic sense, as pointed out previously (*10*). The two fibrils would be convertible when ΔH becomes comparable to $T\Delta S$ because of the structural change in the protein. Actually, however, the conversion is not so free at room temperature (*10*, *39*, *63*), because the contribution from ΔH is large, and therefore, the formation of the hook considerably stabilizes the structure of the LS fibril in this explanation.

The conversion from the WL to LS fibrils does not occur until the side chains of the proteins form hooks in an appropriate way. This is generally difficult and hence only rarely occurs, probably because of the longer distances between the partner residues in the irregular structure. The conversion from the LS to WL fibril is also difficult, because hooks are not easily cleaved once formed. The disulfide bridge between Cys25 and Cys80 should play a critical role in the formation of this hook by allowing the partner residues in the different β-strands to come into the proximity of one another. Therefore, when the disulfide bridge is reduced, the fibril formation property disappears (*8*). The importance of the attractive interaction by the deprotonated carboxyl side chains is also reportedly seen in the case of the amyloid β (1−40) peptide (Aβ_{1-40}); the salt bridge between Asp23 and Lys28 stabilized the stack of β-sheets in the fibril structure of Aβ_{1-40} (*21*), and also the covalent linking of these two residues accelerated the fibril formation 1000-fold (*64*). The Aβ_{1-40} fibrils formed under quiescent and agitated conditions exhibited a morphological difference, and a structural difference was observed in the formation of the salt bridge between Lys16 and Glu22 (*13*).

On the other hand, the salt concentration did not affect the IR spectral feature, i.e., the structures of the K3 and K3−K7 fibrils. The modulation of the pK_a of COOH groups was absent, while the LS morphology was observed (Figure 4c,d). The electrostatic interaction seems to be scarcely important in these cases. These results could be explained in terms of a uniform intermolecular interaction between the peptides, as the number of sites relevant to the intermolecular interaction and the fraction of unordered structures susceptible to the salt are expected to be small in these peptides. These results suggest the robustness of the β-sheet core structure of the β_2m fibrils, because the K3 and K3−K7 fragments are incorporated into the β-sheet core in both the LS and WL fibrils (*59*, *65*).

Then the observed susceptibility of the β_2m fibrils to the salt concentration should be attributed to the β-sheet formation property of other regions besides the β-sheet core; those sequences that appear to have a low propensity for the β-sheet structure could be responsible. This idea agrees with the work of Yamaguchi et al., who suggested that the formation of the β-sheet network, including the loop regions in the native state, is a possible origin of the morphological difference between the LS and WL β_2m fibrils (*65*). In consonance with these results, the minor role of the salt bridges in the stabilization of the protein structure has been revealed; the salt bridge between the Glu-Lys pair is less efficient than the side chain interaction between the Phe-Phe pair in the stabilization of the β-hairpin structure (*66*). Aromatic interaction seems to be crucial instead, as a dipeptide, Phe-Phe, forms a fibrilous construct (*67*). The salt bridge is required to suppress the movement of the unfixed parts, but not to create the strong framework of the β-sheet core (*66*).

Sodium dodecyl sulfate (SDS) yielded the β_2m fibril at neutral pH, but cationic, amphipathic, and nonionic detergents did not exhibit a potency as strong as that of SDS (*4*). This result suggested the importance of the electrostatic interactions between the positively charged residues of β_2m and the negative charges of the sulfonic groups. In relation to this, different potencies of certain anionic species (namely, SO_4^{2-}, ClO_4^-, I^-, and Cl^-) in relation to the fibril formation of β_2m have been reported, in which the importance of the preferential anion binding to the protein was noted (*68*). The role of salts and charged side chains in fibril formation is a subject for future investigation.

With regard to the main chain structure, the β-sheet content was determined to be $53 \pm 6\%$ in the LS fibril and $47 \pm 6\%$ in the WL fibril. These values do not closely agree with the reported results from the H−D exchange experiment (*65*), in which the amount of β-sheet in the LS and WL fibrils was estimated to be ~80 and ~30% of the whole sequence, respectively. These reported findings suggested that the morphology of the fibril having a higher β-sheet content was more directionally oriented, and that the β-sheet content was higher in the LS fibril than in the WL fibril. These results qualitatively agree with this idea; however, the difference was not as large as reported, and further study will be necessary.

Potential sources of error in this analysis include uncertainties in the analytic procedure itself and the uniqueness of the band fittings. The former involves the uncertainty of the empirical knowledge about the peak positions of the amide I band, and the variations of the molar extinction coefficient among secondary structures (*69*). As an example of the worst case, the extinction coefficient of poly(Lys) increases up to 1.3 times upon the transformation from random to β-sheet structure (*70*), and in such a case, the estimation of the number of residues contains the

corresponding errors. Unfortunately, there is no appropriate method for compensation for this at present.

Finally, there is the issue of the β-helix as the core structure of the fibril. One of the possible conformations of the peptide main chain in amyloid fibrils is a helical conformation called the β-helix (*71*), in which dihedral angles ψ and ϕ are classified as the β-strand structure. Indeed, the β-helix has been proposed as the core structure of certain protein fibrils (*71*−*73*). However, the peak frequencies of the amide I bands observed in these Raman spectra (1671 cm^{-1} in the LS fibril and 1670 cm^{-1} in the WL fibril) do not agree with those of the P22 tailspike protein (1667 cm^{-1}), which does contain the β-helix structure (*74*). Since the Raman band is sharp and intense, its error is much smaller than the difference insofar as the frequency calibration is performed carefully. Therefore, the disagreement does not necessarily support the β-helix structure as a universal frame in the case of the β_2m fibrils. It is noted that the IR spectrum of the β-helix structure does not provide a diagnostic band (*75*).

CONCLUSION

The molecular structure of β_2-microglobulin (β_2m) in solution and the fibrils was analyzed by means of IR, Raman, and VUVCD spectroscopy. Distinct differences between the LS and WL fibrils that yield needlelike and flexible morphologies, respectively, were found in the protonated state of the carboxyl side chains; they were predominantly deprotonated even at pH 2.5 in the LS fibril but were protonated in the WL fibril. The lowering of the pK_a of the carboxyl groups suggested the presence of hooklike interactions, such as hydrogen bonding and salt bridge formation, between the COO^- groups and some of the residues in the LS fibril. This could be the origin of the linear morphology of the LS fibril. The β-sheet contents in the LS and WL fibrils were similar (53 ± 6 and 47 ± 6%, respectively) and were comparable with that in the native state (53 ± 6%). Therefore, the secondary structure preference in the fibrils is considered to be similar with each other. A Raman band characteristic of the β-helix was not observed.

ACKNOWLEDGMENT

We are deeply indebted to Dr. Hisashi Yagi of the Institute for Protein Research, Osaka University, for his kind measurements of AFM and TEM images. Pacific Edit reviewed the manuscript prior to submission.

REFERENCES

1. Bjorkman, P. J., Saper, M. A., Samraoui, B., Bennett, W. S., Strominger, J. L., and Wiley, D. C. (1987) Structure of the human class I histocompatibility antigen, HLA-A2. *Nature 329*, 506–512.
2. Morgan, C. J., Gelfand, M., Atreya, C., and Miranker, A. D. (2001) Kidney dialysis-associated amyloidosis: A molecular role for copper in fiber formation. *J. Mol. Biol. 309*, 339–345.
3. Eakin, C. M., Berman, A. J., and Miranker, A. D. (2006) A native to amyloidgenic transition regulated by a backbone trigger. *Nat. Struct. Mol. Biol. 13*, 202–208.
4. Yamamoto, S., Hasegawa, K., Yamaguchi, I., Tsutsumi, S., Kardos, J., Goto, Y., Gejyo, F., and Naiki, H. (2004) Low concentrations of sodium dodecyl sulfate induce the extension of β_2-microglobulin-related amyloid fibrils at neutral pH. *Biochemistry 43*, 11075–11082.
5. Relini, A., Canale, C., Stefano, S. D., Rolandi, R., Giorgetti, S., Stoppini, M., Rossi, A., Fogolari, F., Corazza, A., Esposito, G., Gliozzi, A., and Bellotti, V. (2006) Collagen plays an active role in the aggregation of β_2-microglobulin under physiopathological conditions of dialysis-related amyloidosis. *J. Biol. Chem. 281*, 16521–16529.
6. Relini, A., De Stefano, S., Torrassa, S., Cavalleri, O., Rolandi, R., Gliozzi, A., Giorgetti, S., Raimondi, S., Marchese, L., Verga, L., Rossi, A., Stoppini, M., and Bellotti, V. (2008) Heparin strongly enhances the formation of β_2-microglobulin amyloid fibrils in the presence of type I collagen. *J. Biol. Chem. 283*, 4912–4920.
7. Hasegawa, K., Tsutsumi-Yasuhara, S., Ookoshi, T., Ohhashi, Y., Kimura, H., Takahashi, N., Yoshida, H., Miyazaki, R., Goto, Y., and Naiki, H. (2008) Growth of β_2-microlobulin-related amyloid fibrils by non-esterified fatty acids at a neutral pH. *Biochem. J. 416*, 307–315.
8. Ohhashi, Y., Hagihara, Y., Kozhukh, G., Hoshino, M., Hasegawa, K., Yamaguchi, I., Naiki, H., and Goto, Y. (2002) The intrachain disulfide bond of β_2-microglobulin is not essential for the immunoglobulin fold at neutral pH, but is essential for amyloid fibril formation at acidic pH. *J. Biochem. 131*, 45–52.
9. McParland, V. J., Kad, N. M., Kalverda, A. P., Brown, A., Kirwin-Jones, P., Hunter, M. G., Sunde, M., and Radford, S. E. (2000) Partially unfolded states of β_2-microglobulin and amyloid formation in vitro. *Biochemistry 39*, 8735–8746.
10. Gosal, W. G., Morten, I. J., Hewitt, E. W., Smith, A., Thomson, N. H., and Radford, S. E. (2005) Competing pathways determine fibril morphology in the self-assembly of β_2-microglobulin into amyloid. *J. Mol. Biol. 351*, 850–864.
11. Kad, N. M., Myers, S. L., Smith, D. P., Smith, D. A., Radford, S. E., and Thomson, N. H. (2003) Hierarchical assembly of β_2-microglobulin amyloid in vitro revealed by atomic force microscopy. *J. Mol. Biol. 330*, 785–797.
12. Dobson, C. M. (1999) Protein misfolding, evolution and disease. *Trends Biochem. Sci. 24*, 329–332.
13. Petkova, A. T., Leapman, R. D., Guo, Z., Yau, W.-M., Mattson, M. P., and Tycko, R. (2005) Self-propagating, molecular-level polymorphism in Alzheimer's β-amyloid fibrils. *Science 307*, 262–265.
14. Dong, J., Shokes, J. E., Scott, R. A., and Lynn, D. G. (2006) Modulating amyloid self assembly and fibril morphology with Zn(II). *J. Am. Chem. Soc. 128*, 3540–3542.
15. Hoyer, W., Antony, T., Cherny, D., Heim, G., Jovin, T. M., and Subramaniam, V. (2002) Dependence of α-synuclein aggregate morphology on solution conditions. *J. Mol. Biol. 322*, 383–393.
16. Zerovnik, E., Skarabot, M., Skerget, K., Giannini, S., Stoka, V., Jenko-Kokalj, S., and Staniforth, R. A. (2007) Amyloid fibril formation by human stefin B: Influence of pH and TFE on fibril growth and morphology. *Amyloid 14*, 237–247.
17. Goldsbury, C., Kistler, J., Aebi, U., Arvinte, T., and Cooper, G. J. S. (1999) Watching amyloid fibrils grow by time-lapse atomic force microscopy. *J. Mol. Biol. 285*, 33–39.
18. Jimenez, J. L., Nettleton, E. J., Bouchard, M., Robinson, C. V., Dobson, C. M., and Saibil, H. R. (2002) The protofilament structure of insulin amyloid fibrils. *Proc. Natl. Acad. Sci. U.S.A. 99*, 9196–9201.
19. Ban, T., Yamaguchi, K., and Goto, Y. (2006) Direct observation of amyloid fibril growth, propagation, and adaptation. *Acc. Chem. Res. 39*, 663–670.
20. Ban, T., Hoshino, M., Takahashi, S., Hamada, D., Hasegawa, K., Naiki, H., and Goto, Y. (2004) Direct observation of Aβ amyloid fibril growth and inhibition. *J. Mol. Biol. 344*, 757–767.
21. Petkova, A. T., Ishii, Y., Balbach, J. J., Antzutkin, O. N., Leapman, R. D., Delaglio, F., and Tycko, R. (2002) A structural model for Alzheimer's β-amyloid fibrils based on experimental constraints from solid state NMR. *Proc. Natl. Acad. Sci. U.S.A. 99*, 16742–16747.
22. Jaroniec, C. P., MacPhee, C. E., Bajaj, V. S., McMahon, M. T., Dobson, C. M., and Griffin, R. G. (2004) High-resolution molecular structure of a peptide in an amyloid fibril determined by magic angle spinning NMR spectroscopy. *Proc. Natl. Acad. Sci. U.S.A. 101*, 711–716.
23. Makin, O. S., Atkins, E., Sikorski, P., Johansson, J., and Serpell, L. C. (2005) Molecular basis for amyloid fibril formation and stability. *Proc. Natl. Acad. Sci. U.S.A. 102*, 315–320.
24. Iwata, K., Fujiwara, T., Matsuki, Y., Akutsu, H., Takahashi, S., Naiki, H., and Goto, Y. (2006) 3D structure of amyloid protofilaments of β_2-microglobulin fragment probed by solid-stated NMR. *Proc. Natl. Acad. Sci. U.S.A. 103*, 18119–18124.
25. Byler, D. M., and Susi, H. (1986) Examination of the secondary structure of proteins by deconvolved FTIR spectra. *Biopolymers 25*, 469–487.
26. Dong, A., Huang, P., and Caughey, W. S. (1990) Protein secondary structures in water from second-derivative amide I infrared spectra. *Biochemistry 29*, 3303–3308.
27. Kitagawa, T., Azuma, T., and Hamaguchi, K. (1979) The Raman spectra of Bence-Jones proteins. Disulfide stretching frequencies and dependence of Raman intensity of tryptophan residues on their environments. *Biopolymers 18*, 451–465.
28. Williams, R. W. (1983) Estimation of protein secondary structure from the laser Raman amide I spectrum. *J. Mol. Biol. 166*, 581–603.

29. Naumann, D. (2001) FT-infrared and FT-Raman spectroscopy in biomedical research. *Appl. Spectrosc. Rev. 36*, 239–298.
30. Barth, A., and Zscherp, C. (2002) What vibrations tell us about proteins. *Q. Rev. Biophys. 35*, 368–430.
31. Baena, J. R., and Lendl, B. (2004) Raman spectroscopy in chemical bioanalysis. *Curr. Opin. Chem. Biol. 8*, 534–539.
32. Paul, C., Wang, J., Wimley, W. C., Hochstrasser, R. M., and Axelsen, P. H. (2004) Vibrational coupling, isotope editing, and β-sheet structure in a membrane-bound polypeptide. *J. Am. Chem. Soc. 126*, 5843–5850.
33. Hiramatsu, H., Goto, Y., and Kitagawa, T. (2005) Structural model of the amyloid fibril formed by β_2-microglobulin #21−31 fragment based on vibrational spectroscopy. *J. Am. Chem. Soc. 127*, 7988–7989.
34. Lu, M., Hiramatsu, H., Goto, Y., and Kitagawa, T. (2006) Structure of interacting segments in the growing amyloid fibril of β_2-microglobulin probed with IR spectroscopy. *J. Mol. Biol. 362*, 355–364.
35. Hiramatsu, H., Goto, Y., Naiki, H., and Kitagawa, T. (2004) Core structure of amyloid fibril proposed from IR-microscope linear dichloism. *J. Am. Chem. Soc. 126*, 3008–3009.
36. Sreerama, N., and Woody, R. W. (2000) Estimation of protein secondary structure from circular dichroism spectra: Comparison of CONTIN, SELCON, and CDSSTR methods with an expanded reference set. *Anal. Biochem. 287*, 252–260.
37. Jahn, T. R., Tennent, G. A., and Radford, S. E. (2008) A common β-sheet architecture underlies in vitro and in vivo β_2-microglobulin amyloid fibrils. *J. Biol. Chem. 283*, 17279–17286.
38. Fabian, H., Gast, K., Laue, M., Misselwitz, R., Uchanska-Ziegler, B., Ziegler, A., and Naumann, D. (2008) Early stages of misfolding and association of β_2-microglobulin: Insights from infrared spectroscopy and dynamic light scattering. *Biochemistry 47*, 6895–6906.
39. Hong, D. P., Gozu, M., Hasegawa, K., Naiki, H., and Goto, Y. (2002) Conformation of β_2-microglobulin amyloid fibrils analyzed by reduction of the disulfide bond. *J. Biol. Chem. 277*, 21554–21560.
40. Kozhukh, G. V., Hagihara, Y., Kawakami, T., Hasegawa, K., Naiki, H., and Goto, Y. (2002) Investigation of a peptide responsible for amyloid fibril formation of β_2-microglobulin by achromobacter protease I*. *J. Biol. Chem. 277*, 1310–1315.
41. Fraser, R. D. B. (1953) The interpretation of infrared dichroism in fibrous protein structures. *J. Chem. Phys. 21*, 1511–1515.
42. Hiramatsu, H., and Kitagawa, T. (2005) FT-IR approaches on amyloid fibril structure. *Biochim. Biophys. Acta 1753*, 100–107.
43. Ojima, N., Sakai, K., Matsuo, K., Matsui, T., Fukazawa, T., Namatame, H., Taniguchi, M., and Gekko, K. (2001) Vacuum-ultraviolet circular dichroism spectrophotometer using synchrotron radiation: Optical system and on-line performance. *Chem. Lett. 30*, 522–523.
44. Matsuo, K., Sakai, K., Matsushima, Y., Fukuyama, T., and Gekko, K. (2003) Optical cell with a temperature-control unit for a vacuum-ultraviolet circular dichroism spectrophotometer. *Anal. Sci. 19*, 129–132.
45. Matsuo, K., Yonehara, R., and Gekko, K. (2004) Secondary-structure analysis of proteins by vacuum-ultraviolet circular dichroism spectroscopy. *J. Biochem. 135*, 405–411.
46. Matsuo, K., Yonehara, R., and Gekko, K. (2005) Improved estimation of the secondary structures of proteins by vacuum-ultraviolet circular dichroism spectroscopy. *J. Biochem. 138*, 79–88.
47. Kabsch, W., and Sander, C. (1983) Dictionary of protein secondary structure: Pattern recognition of hydrogen bonded and geometric feature. *Biopolymers 22*, 2577–2637.
48. Sreerama, N., Venyaminov, S. Y., and Woody, R. W. (1999) Estimation of the number of α-helical and β-strand segments in proteins using circular dichroism spectroscopy. *Protein Sci. 8*, 370–380.
49. Azuma, T., Kobayashi, O., Goto, Y., and Hamaguchi, K. (1978) Monomer-dimer equilibria of a Bence-Jones protein and its variable fragment. *J. Biochem. 83*, 1485–1492.
50. Gorga, J. C., Dong, A., Manning, M. C., Woody, R. W., Caughey, W. S., and Strominger, J. L. (1989) Comparison of the secondary structures of human class I and class II major histocompatibility complex antigenns by Fourier transform infrared and circular dichroism spectroscopy. *Proc. Natl. Acad. Sci. U.S.A. 86*, 2321–2325.
51. McParland, V. J., Kalverda, A. P., Homans, S. W., and Radford, S. E. (2002) Structural properties of an amyloid precursor of β_2-microglobulin. *Nat. Struct. Biol. 9*, 326–331.
52. Katou, H., Kanno, T., Hoshino, M., Hagihara, Y., Tanaka, H., Kawai, T., Hasegawa, K., Naiki, H., and Goto, Y. (2002) The role of disulfide bond in the amyloidogenic state of β_2-microglobulin studied by heteronuclear NMR. *Protein Sci. 11*, 2218–2229.
53. Venyaminov, S. Y., and Kalnin, N. N. (1990) Quantitative IR spectrophotometry of peptide compounds in water (H_2O) solutions. I. Spectral parameters of amino acid residue absorption bands. *Biopolymers 30*, 1243–1257.
54. Lord, R. C., and Yu, N.-T. (1970) Laser-excited Raman spectroscopy of biomolecules. *J. Mol. Biol. 50*, 509–524.
55. Forsyth, W. R., Antosiewicz, J. M., and Robertson, A. D. (2002) Empirical relationships between protein structure and carboxyl pK_a values in proteins. *Proteins 48*, 388–403.
56. Chen, M. C., Lord, R. C., and Mendelsohn, R. (1973) Laser-excited Raman spectroscopy of biomolecules IV. Thermal denaturation of aqueous lysozyme. *Biochim. Biophys. Acta 328*, 252–260.
57. Siamwiza, M. N., Lord, R. C., Chen, M. C., Takamatsu, T., Harada, I., Matsuura, H., and Shimanouchi, T. (1975) Interpretation of the doublet at 850−830 cm^{-1} in the Raman spectra of tyrosyl residues in proteins and certain model compounds. *Biochemistry 14*, 4870–4876.
58. Uegaki, K., Nakamura, T., Yamamoto, H., Kobayashi, A., Odahara, T., Harata, K., Hagihara, Y., Ueyama, N., Yamazaki, T., and Yumoto, N. (2005) Amyloid fibril formation by the CAD domain of caspase-activated DNase. *Biopolymers 79*, 39–47.
59. Hoshino, M., Katou, H., Hagihara, Y., Hasegawa, K., Naiki, H., and Goto, Y. (2002) Mapping the core of the β_2-microglobulin amyloid fibril by H/D exchange. *Nat. Struct. Biol. 9*, 332–336.
60. Krimm, S., and Bandekar, J. (1983) Vibrational spectroscopy and conformation of peptides, polypeptides, and proteins. *Adv. Protein Chem. 38*, 181–364.
61. Oliveberg, M., Arcus, V. L., and Fersht, A. R. (1995) pK_a values of carboxyl groups in the native and denatured states of barnase: The pK_a values of the denatured stated are on average 0.4 units lower than those of model compounds. *Biochemistry 34*, 9424–9433.
62. Oda, Y., Yamazaki, T., Nagayama, K., Kanaya, S., Kuroda, Y., and Nakamura, H. (1994) Individual ionization constants of all the carboxyl groups in ribonuclease HI from *Escherichia coli* determined by NMR. *Biochemistry 33*, 5275–5284.
63. Kad, N. M., Thomson, N. H., Smith, D. P., Smith, D. A., and Radford, S. E. (2001) β_2-Microglobulin and its deamidated variant, N17D, form amyloid fibrils with a range of morphologies in vitro. *J. Mol. Biol. 313*, 559–571.
64. Sciarretta, K. L., Gordon, D. J., Petkova, A. T., Tycko, R., and Meredith, S. C. (2005) Aβ40-lactam(D23/K28) models a conformation highly favorable for nucleation of amyloid. *Biochemistry 44*, 6003–6014.
65. Yamaguchi, K., Katou, H., Hoshino, M., Hasegawa, K., Naiki, H., and Goto, Y. (2004) Core and heterogeneity of β_2-microglobulin amyloid fibrils as revealed by H/D exchange. *J. Mol. Biol. 338*, 559–571.
66. Kiehna, S. E., and Waters, M. L. (2003) Sequence dependence of β-hairpin structure: Comparison of a salt bridge and an aromatic interaction. *Protein Sci. 12*, 2657–2667.
67. Reches, M., and Gazit, E. (2003) Casting metal nanowires within discrete self-assembled peptide nanotubes. *Science 300*, 625–627.
68. Raman, B., Chatani, E., Kihara, M., Ban, T., Sakai, M., Hasegawa, K., Naiki, H., Rao, C. M., and Goto, Y. (2005) Critical balance of electrostatic and hydrophobic interactions is required for β_2-microglobulin amyloid fibril growth and stability. *Biochemistry 44*, 1288–1299.
69. Surewicz, W. K., Mantsch, H. H., and Chapman, D. (1993) Determination of protein secondary structure by Fourier transform infrared spectroscopy: A critical assessment. *Biochemistry 32*, 389–394.
70. Jackson, M., Haris, P. I., and Chapman, D. (1989) Conformational transitions in poly(L-lysine): Studies using Fourier transform infrared spectroscopy. *Biochim. Biophys. Acta 998*, 75–79.
71. Perutz, M. F., Finch, J. T., Berriman, J., and Lesk, A. (2002) Amyloid fibers are water-filled nanotubes. *Proc. Natl. Acad. Sci. U.S.A. 99*, 5591–5595.
72. Margittai, M., and Langen, R. (2004) Template-assisted filament growth by parallel stacking of tau. *Proc. Natl. Acad. Sci. U.S.A. 101*, 10278–10283.
73. Makin, O. S., and Serpell, L. C. (2005) Structures for amyloid fibrils. *FEBS J. 272*, 5950–5961.
74. Raso, S. W., Clark, P. L., Haase-Pettingell, C., King, J., and Thomas, G. J., Jr. (2001) Distinct cysteine sulfhydryl environments detected by analysis of Raman S-H markers of Cys → Ser mutant proteins. *J. Mol. Biol. 307*, 899–911.
75. Khurana, R., and Fink, A. L. (2000) Do parallel β-helix proteins have a unique Fourier transform infrared spectrum? *Biophys. J. 78*, 994–1000.